International Journal of Greenhouse Gas Control 33 (2015) 27–39

Contents lists available at ScienceDirect

International Journal of Greenhouse Gas Control

journal homepage: www.elsevier.com/locate/ijggc

A response surface model to predict CO_2 and brine leakage along cemented wellbores

Amy B. Jordan*, Philip H. Stauffer, Dylan Harp, J. William Carey, Rajesh J. Pawar

Earth and Environmental Sciences Division, Los Alamos National Laboratory, Computational Earth Sciences Group, EES-16, MS T003, Los Alamos, 87545 NM, United States

ARTICLE INFO

Article history:
Received 28 May 2014
Received in revised form 7 November 2014
Accepted 3 December 2014

Keywords:
Sequestration
Carbon storage
Wellbore leakage
System-scale modeling
Probabilistic risk analysis

ABSTRACT

Potential CO_2 and brine leakage from geologic sequestration reservoirs must be quantified on a site-specific basis to predict the long-term effectiveness of geologic storage. The primary goals of this study are to develop and validate reduced-order models (ROMs) to estimate wellbore leakage rates of CO_2 and brine from storage reservoirs to the surface or into overlying aquifers, and to understand how the leakage profile evolves as a function of wellbore properties and the state of the CO_2 plume. A multiphase reservoir simulator is used to perform Monte Carlo simulations of CO_2 and water flow along wellbores across a wide range of relevant parameters including wellbore permeability, wellbore depth, reservoir pressure and saturation. The leakage rates are used to produce validated response surfaces that can be sampled to estimate wellbore flow. Minima in flow rates seen in the response surface are shown to result from complex nonlinear phase behavior along the wellbore. Presence of a shallow aquifer can increase CO_2 leakage compared to cases that only allow CO_2 flow directly to the land surface. The response surfaces are converted into computationally efficient ROMs and the utility of the ROMs is demonstrated by incorporation into a system-level risk analysis tool.

© 2014 Elsevier Ltd. All rights reserved.

1. Introduction

Geologic carbon sequestration (GCS) has been proposed as a means to reduce the amount of CO_2 added annually to the atmospheric carbon budget (Metz et al., 2005). Sites with the potential for significant CO_2 storage include saline reservoirs and depleted oil and gas-bearing formations, coal beds, and salt caverns (Bachu, 2000). There are several benefits to using reservoirs that have already been tapped for hydrocarbon production as compared to undeveloped sites: they tend to be geologically well-understood, with existing wellbore data to help characterize the local geology; are known to trap buoyant or pressurized fluids; and may already have infrastructure in place. One downside to using depleted hydrocarbon reservoirs is the presence of pre-existing wells (Gasda et al., 2004). This creates an increased potential (as compared with undeveloped sites) for CO_2 and brine leakage to the surface or to drinking water aquifers. In order to provide a comprehensive assessment of the risks and performance of large-scale GCS scenarios, the estimation of CO_2 and brine leakage along wellbores is essential.

Preferential pathways for wellbore CO_2 leakage may include flow through degraded cement and flow along cracks and interfaces between materials (Gasda et al., 2004; Carey, 2013). Actual geometries of permeable pathways produced by wellbore degradation will be unknown for the multitude of wellbores across a regional-scale GCS site. Treating the wellbore as an equivalent Darcy medium with an overall "effective permeability" is one approach to bundling uncertainty in wellbore architecture in order to estimate wellbore flow rates (e.g., Gasda et al., 2008; Crow et al., 2010; Brunet et al., 2013).

Another approach to modeling CO_2 leakage is with a drift flux model. Pan et al. (2011) developed an analytical model for 1-D multiphase flow based on this approach. Hu et al. (2012) compare the drift flux model to treating the open wellbore as an equivalent Darcy medium with high permeability and porosity, and find the equivalent Darcy approach is less reliable at high leakage rates (greater than approximately 20 kg/s). The wellbore leakage model presented here does not cover open boreholes with leak rates of those magnitudes.

High-fidelity, multiphase reservoir numerical simulation of CO_2 and brine leakage through multiple wellbores across the large spatial and temporal scales of GCS operations is computationally expensive. Thus, in order to quickly estimate wellbore leakage within a risk assessment framework, reduced-order models (ROMs) that allow a probabilistic treatment of unknown parameters have

* Corresponding author. Tel.: +1 505 667 1049; fax: +1 505 665 6459.
E-mail address: ajordan@lanl.gov (A.B. Jordan).

http://dx.doi.org/10.1016/j.ijggc.2014.12.002
1750-5836/© 2014 Elsevier Ltd. All rights reserved.

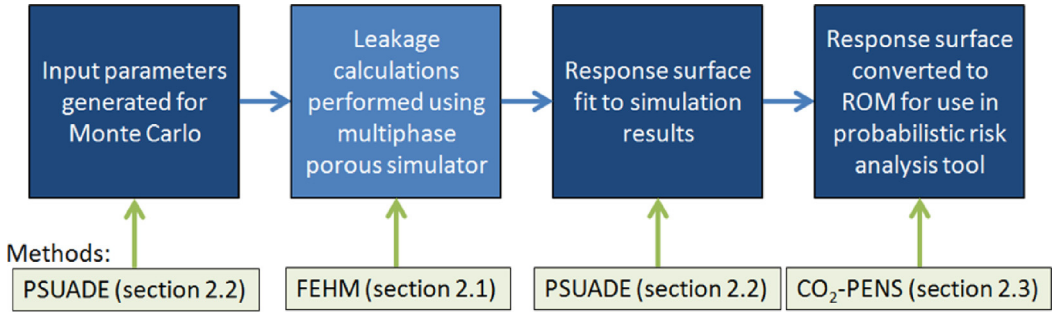

Fig. 1. Workflow for the response surface development and implementation.

been sought (Viswanathan et al., 2008; Celia and Nordbotten, 2011; Nordbotten et al., 2009).

In this paper, we describe a method for creating wellbore leakage response surfaces based on thousands of multiphase porous flow simulations. The resulting validated wellbore leakage response surfaces are built into reduced-order models (ROMs) that calculate both CO_2 and water leakage when sampled from multiple factors that drive flow, such as reservoir depth, effective wellbore permeability, bottom hole pressure and CO_2 saturation, and whether the flow is directly to the atmosphere or into an overlying shallow aquifer. Analysis of the leakage rates versus controlling parameters reveals minima created by nonlinear phase change within the wellbore. The ROMs allow uncertain values of controlling parameters to be sampled rapidly for use in risk analysis. Finally, to demonstrate the utility of the ROMs in risk analysis, the wellbore leakage ROMs are coupled into the system-level analysis tool CO_2-PENS (predicting engineered natural systems) (Stauffer et al., 2009; Pawar et al., 2013) and results for a hypothetical GCS site are presented. To date, these ROMs have been used in CO_2-PENS (Pawar et al., 2013) and in other risk assessment frameworks for GCS sites (Dai et al., 2014).

2. Methods

To create ROMs for wellbore leakage in two scenarios (with and without an overlying aquifer), a total of 1500 simulations are performed using a multiphase porous flow simulator. The workflow for producing the ROMs involves linking four numerical components (Fig. 1). A Latin hypercube sampling (LHS) scheme is used to efficiently sample the 5-D parameter space: (1) effective wellbore permeability, (2) reservoir depth, (3) reservoir pressure and (4) CO_2 saturation at the bottom of the wellbore, and (5) residual saturation of water. We then calculate the wellbore leakage of both CO_2 and water in 2-D radial coordinates as an equivalent Darcy medium. Next, a response surface is generated that links input parameters to CO_2 and water leakage rates. The response surface is then integrated into CO_2-PENS as a wellbore leakage ROM and an example calculation using a hypothetical GCS site is shown to demonstrate the utility of the ROM.

Wellbore leakage simulations were conducted with the finite element heat and mass (FEHM) code (Section 2.1), which handles multiphase, non-isothermal flow using the control volume finite element method (Zyvoloski, 2007). The Monte Carlo variation of parameters and ROM production using statistical software is described in Section 2.2. The GCS performance assessment model CO_2-PENS is discussed in Section 2.3.

2.1. Multiphase porous flow simulations

FEHM (fehm.lanl.gov) solves the governing equations of mass and energy conservation, assuming Darcy's Law is applicable for all phases. FEHM has the ability to simulate complex thermodynamics associated with phase change of CO_2 from supercritical to 2-phase to gas as it migrates from deep sequestration reservoirs to the shallow aquifer and atmosphere (Zyvoloski, 2007). Phase properties such as viscosity, density, and enthalpy of CO_2 are computed from a lookup table fit to the National Institute of Standards and Technology (NIST) thermophysical properties database (Linstrom and Mallard, 2014). Publications using FEHM for GCS include the impacts of heterogeneity during industrial scale CO_2 injection (Deng et al., 2012), geomechanical coupling to CO_2 injection (Dempsey et al., 2014), and analysis of linking multiple CO_2 sources to multiple reservoirs for the Southern U.S. (Middleton et al., 2012). To ensure software quality control, FEHM is regularly benchmarked against a suite of test problems provided in Dash (2003).

Two cases are simulated in FEHM: (1) a wellbore, with no intersecting aquifers, with fixed atmospheric pressure at the top; and (2) a wellbore intersecting a 500-m thick aquifer, with CO_2 and water flow allowed at the far-field vertical boundary of the aquifer with lateral constant-pressure boundary conditions (hydrostatic). The geometry and computational mesh for one wellbore leakage simulation for Case 2 (with overlying aquifer) is shown in Fig. 2. All caprock material is impermeable, but is included in the model to account for the heat transfer associated with phase change of CO_2 during leakage.

Pressure at the CO_2 leak point is held constant at a value related to the lithostatic overburden pressure at the bottom wellbore depth:

$$CO_2 \quad \text{pressure} = [\rho_r(1-\phi) + \rho_w\phi]\, gD \times \Pi \tag{1}$$

where ρ_r and ρ_w are the rock grain density and water density, ϕ is porosity, g is acceleration due to gravity, D is wellbore depth, and Π is a parameter defining the fraction of lithostatic pressure. Pressure is given in terms of a fraction of lithostatic overburden because the amount of overpressure the rock can sustain without failure increases with depth; CO_2 may be injected under higher pressures at deeper depths (Stauffer et al., 2009). Note that care should be taken to distinguish between absolute CO_2 pressure (P, in MPa); pressure as a fraction of lithostatic (dimensionless Π); and two other measures of excess pressure, EPP and EPP^*, used and defined in Section 4.1.

Boundary conditions for the simulations are fixed water pressure, CO_2 pressure (P), and saturation (C) at the leak point, with CO_2 and water flow allowed at this point; and, for Case 2 with an aquifer, CO_2 and water flow allowed out of the far-field boundary of the upper aquifer (2000 m), with pressures fixed to initial hydrostatic values. At the top wellbore boundary, pressure for all phases is fixed to atmospheric (0.1 MPa). The temperature of incoming CO_2 at the leak point is the same as water at that depth, based on a geothermal gradient of 30 °C/km.

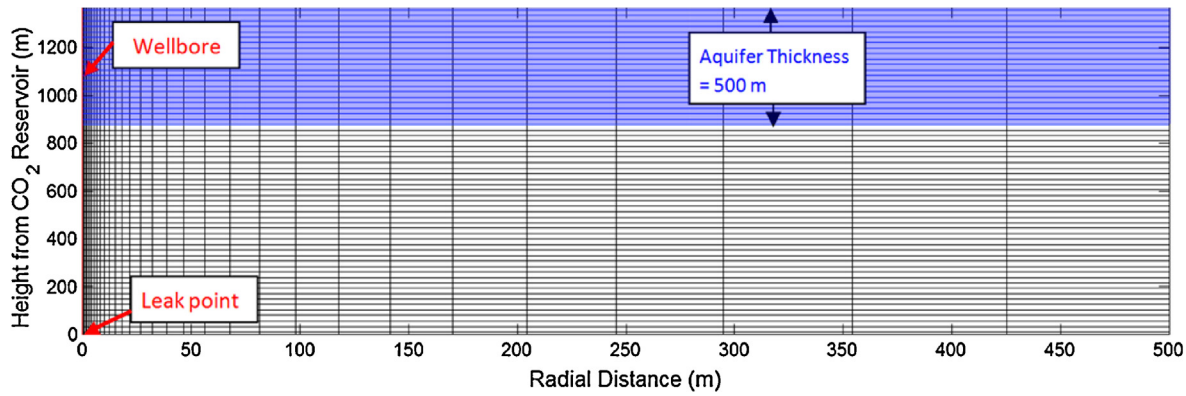

Fig. 2. Computational mesh layout for one Case 2 realization (leak point depth of 1368 m). An impermeable caprock extends from 1368 to 500 m below ground surface, with a higher permeability (1 D) aquifer from 500 m to the surface. The computational mesh extends to 2000 m radial distance. The CO_2 reservoir is not explicitly modeled; a node at the bottom left of the domain (the leak point) has boundary conditions representing fixed pressure and CO_2 saturation in the reservoir where it is intersected by a wellbore.

We have not included CO_2 dissolution in reservoir brine and other reactive chemistry (e.g., Viswanathan et al., 2012; Balashov et al., 2013), as well as geomechanical and geochemical alterations to the medium as a result of interaction between CO_2 and cement (Carey, 2013; Dempsey et al., 2014). These are assumed to be second-order effects and are not included in this version of the ROM. Other simplifications include the use of homogeneous wellbore properties instead of representing likely zones of permeability throughout the wellbore, e.g., greater permeability reduction closest to the CO_2 reservoir (Crow et al., 2010). The model assumes a geothermal gradient of 30 °C/km and a linear model for relative permeability of CO_2 and water. The linear model is chosen because the response surface will be applied to widely varying sites with potentially limited available relative permeability data. The linear model will also allow for a conservative possible leak rate estimation. It is assumed that there are no "thief zones," or intervening aquifers between the surface or upper 500 m thick aquifer (the two cases tested). Although thief zones could potentially divert CO_2 from the wellbore and can significantly reduce leakage (Nordbotten et al., 2004), they are not included here for this first-generation implementation of the ROM. Future work will focus on the impact of thief zones on wellbore leakage.

In this analysis we do not seek to address the nature of the wellbore leakage; we simply assume that there is some effective permeability to the wellbore system and that flow is determined by a multiphase form of Darcy's Law. The system-level model into which the wellbore leakage ROMs are incorporated includes uncertainty in the wellbore effective permeability due to the nature of the preferential pathway to flow (Viswanathan et al., 2008). The assumption of Darcy flow in the wellbore is reasonable for leakage through wellbore cement but not necessarily for open spaces in the wells such as annular regions between casings or between the casing and rock (Pan et al., 2009). We include very high-permeability wellbore calculations to represent an equivalent Darcy approach to modeling these regions, but these are not meant to capture the physics of flow through an open annulus or open-pipe, only to provide an approximation that may be valid for the types of variable wellbore degradation expected (Birkholzer et al., 2011a). Alternative modeling approaches for this type of leakage could be used in conjunction with the method presented here for Darcy flow leakage through intact or degraded wellbore cement (Pan et al., 2011).

After conversion to ROMs, the response surfaces are intended to be used in CO_2-PENS during active injection or post-injection periods. Once the permeability of the wellbore is assigned during model initiation, the only parameters needed to estimate a wellbore leakage are the time-varying pressure and CO_2 saturation at the base of the wellbore. Although the response surfaces are produced using steady-state leakage results with long-term (10 year) fixed pressure/saturation boundary conditions, the response surfaces are developed for use within transient simulations where pressures and CO_2 saturation could change continuously. However, because timescales for plume migration are generally much larger than timescales for wellbore leakage (Celia and Nordbotten, 2011), the use of steady-state runs is reasonable for a first-order leakage estimate. Because the sequestration reservoir is not explicitly modeled, we do not include the effects of changing pressure and CO_2 saturation due to leakage when computing steady-state leakage rates. Typically, the amount leaked is small compared to the amount injected, and the corresponding effects on pressure and saturation would be expected to be minimal.

We do not consider salinity of the leaking water, but Hu et al. (2012) quantify the impact of salinity on brine leakage rates in an open wellbore. Salinity and salinity gradient primarily affect wellbore flow due to density differences, but Bachu and Bennion (2008, 2009) show that salinity may also be an important factor in altering retention curves for relative permeability in reservoirs.

While this first-generation model has the features and simplifications described above, the method can easily be adapted to include additional complexity, such as: varying aquifer geometries, different relative permeability functions, different geothermal gradients, wellbore size and length, salinity, and choice of boundary conditions.

2.2. Monte Carlo simulations

The problem solving environment for uncertainty analysis and design exploration (PSUADE) software provides tools for designing Monte Carlo schemes, for fitting models to simulation results, and for analyzing sensitivity of the results to the varied parameters (Tong, 2010). We use PSUADE to generate input parameters for our leakage model; these parameters are then used in multiple realizations of wellbore leakage using the FEHM simulator, and finally PSUADE is used to analyze the FEHM simulation output and produce a response surface, as discussed below.

Parameter distributions were generated for the Monte Carlo realizations using a Latin hypercube sampling scheme in PSUADE, with the ranges of parameters used in the simulations given in Table 1. Wellbore permeability (k) was sampled from a uniform distribution of log (k). Depth (D), Π, C, and residual water saturation (S_{wr}) were drawn from uniform distributions. Because flow rate is directly proportional to wellbore cross-sectional area available for flow, the flow rate should be multiplied by the ratio of the wellbore area of interest divided by the wellbore area used to produce the response surface.

Table 1
Ranges of variable parameters (shaded) and values of fixed parameters used in the wellbore leakage simulations.

Parameter	Value or range
Depth to top of reservoir, m below ground surface (D)	1000–4000
Wellbore permeability (k), m^2	1×10^{-14}–1×10^{-10} (0.01–100 D)
Pressure, fraction of lithostatic (Π) (Eq. (1))	0.485–0.90
CO_2 saturation (C)	0.01–1.0
Residual water saturation (S_{wr})	0–0.35
Wellbore diameter (cm)	10
Wellbore porosity	0.1
Aquifer permeability (m^2)	1×10^{-12} (1 D)
Aquifer porosity	0.1
Aquifer thickness (m)	500
Thermal gradient	30 °C/km
Surface temperature	20 °C
Rock density (kg/m^3)	2200

The reported range of effective permeabilities for wellbores is quite large, from good cement to degraded (but intact) cement to fractured material. Cement alteration due to the presence of CO_2 at high concentrations has been studied for a natural CO_2 production system (Crow et al., 2010) and an enhanced oil recovery site (Carey et al., 2007). Degraded cement in one field study exhibited a maximum permeability of 3.2×10^{-17} m^2 (0.032 mD) (Crow et al., 2010), and alteration attenuated rapidly with distance from the CO_2 reservoir, indicating that the cement remained an effective barrier to CO_2 migration despite near-reservoir alteration. This same study also found that the effective permeability of the cement plus interfaces (obtained using a vertical interference test) was about 1×10^{-15} m^2 (1 mD). On the other hand, a 1-mm annulus located at an interface of well materials would correspond to an effective permeability of $\sim 8 \times 10^{-11}$ m^2 (80 D), using a cubic law for effective permeability for flow parallel to the annulus as a function of aperture size (Viswanathan et al., 2008). The field-measured values of permeabilities for degraded cement produce extremely low CO_2 leakage rates ($\sim 10^{-5}$ t/yr for 3.2×10^{-17} m^2 [0.032 mD]). However, to account for leakage risks due to higher permeability which may result due to annular pathways, cracks, or highly damaged materials (e.g., debris) we use the higher range of wellbore permeability as noted in Table 1. These high-permeability values are used to accurately populate the ROM, but may be user-defined to have low probability of occurrence in the probabilistic risk analysis model. The choice of overpressures of CO_2 at the leak point span from nearly hydrostatic (e.g., a slight overpressure at the far edge of a CO_2 plume as it comes into contact with a wellbore—$\Pi = 0.485$) to highly over pressured (e.g., near the point of injection). Based on hydrofracture considerations, CO_2 is unlikely to be injected at pressures greater than 65–80% of lithostatic (Stauffer et al., 2009), but the response surfaces allow in-situ pressures of up to 90% of lithostatic ($\Pi = 0.9$).

The residual liquid saturation of the node at the point of contact between wellbore and the CO_2 reservoir (not explicitly represented in the computational mesh) is set to 0, to allow cases where the randomly sampled CO_2 saturation at the leak point may be higher than $1 - S_{wr}$.

Using the input parameters determined in PSUADE, FEHM simulations are performed to calculate CO_2 and water flow rate up the wellbore, initially containing 100% water, for 1500 cases with varying D, k, Π, C, and S_{wr}. Steady-state flow rates for CO_2 and water up the wellbore were then analyzed using PSUADE to produce response surfaces as a function of the varied parameters. It was immediately observed that any attempt to fit a multi-dimensional regression to the leakage results would fail, due to the nonlinear and non-monotonic response of leakage to the input parameters. Therefore, the response surfaces were generated in PSUADE using a multivariate adaptive regression spline (MARS) fitting algorithm (Friedman, 1991; Tong, 2010).

The MARS method is an efficient spline-fitting algorithm for multivariate response surface production. A MARS-based response surface can be described in terms of basis or "hinge" functions, which apply from one "knot" or location to another. The basis functions take the form (e.g., Yang et al., 2003):

$$\begin{aligned} Y_i &= \max\ (0,\quad X - c_i) \times Y_j, \quad X > c_i \\ Y_i &= \max\ (0,\quad c_i - X) \times Y_j, \quad X < c_i \end{aligned} \tag{2}$$

where Y_i is the output from basis function i, X is the input variable, c_i is a constant for each basis function, and Y_j is another basis function (basis functions may multiply each other; $Y_0 = 1$ may also be an option where Y_i is not multiplied by any other basis function). The final output is

$$O = a + \sum_i (k_i \times Y_i), \tag{3}$$

where a is a constant for when the output of all basis functions is zero and k_i is a constant for each individual basis function. The procedure for optimizing the MARS method and determining knot locations is described in Friedman (1991) and Yang et al. (2003). Coefficients and basis equations from the response surfaces produced here for wellbore leakage can be provided by contacting the corresponding author.

2.3. Probabilistic risk analysis tool

CO_2-PENS is a system-level probabilistic risk analysis tool for carbon capture and storage which has been used to analyze GCS performance and risk (Stauffer et al., 2009; Pawar et al., 2013) as well as contribute to models of GCS cost and efficiency (Middleton et al., 2012). The CO_2-PENS platform brings together process-scale models in an adaptable, modular format. The modules may be analytical formulations of process models, such as the CO_2 plume evolution formulation of Nordbotten et al. (2005) or injectivity (Stauffer et al., 2009); or the modules may be lookup tables. The wellbore leakage response surfaces presented in this paper are implemented as lookup tables (ROMs) in CO_2-PENS based on the MARS best-fits developed in PSAUDE from the FEHM simulation results. Users have the ability in CO_2-PENS to stochastically quantify CO_2 leakage from a field of wellbores with uncertain properties across a GCS site, to analyze risks associated with CO_2 leakage to the atmosphere (Pawar et al., 2013), or to drinking water resources (Dai et al., 2014).

3. Results

3.1. Flow to the surface

Response surfaces for CO_2 and water leakage to the atmosphere are given in Fig. 3. The impact of depth, wellbore permeability, and CO_2 saturation on CO_2 and water leakage rates are represented on a 3-D surface; surfaces for two different injection pressures (as Π, the fraction of lithostatic pressure) are shown. The residual water saturation exerts only a small effect on leakage rate compared to the other four parameters and is not presented as a variable in the response surfaces. Permeability, while sampled from a logarithmic distribution, is displayed linearly in order to effectively demonstrate the nonlinear effects of the varied parameters on flow rate. Flow rates for permeabilities below 1 D are of order 10^{-5} to 10^{-4} kg/s (300–3000 kg/yr).

As expected, higher permeability and higher CO_2 saturation generally result in higher leakage rates. Depth has a distinct impact on

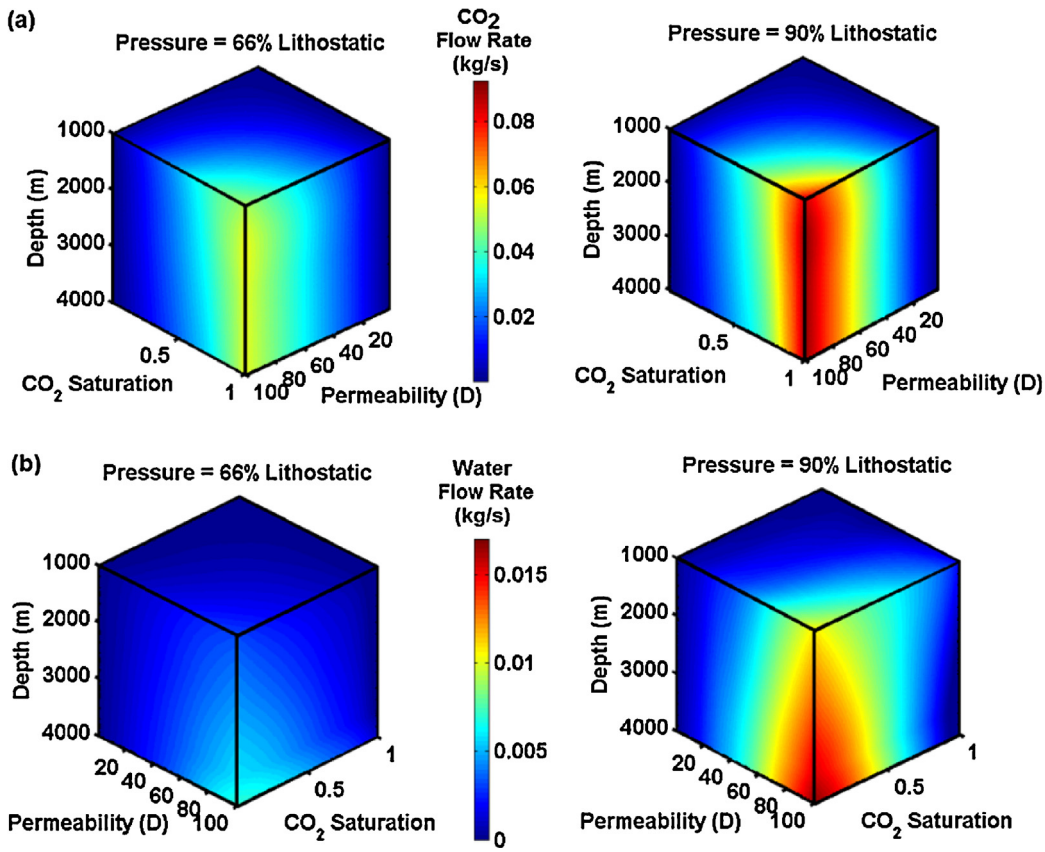

Fig. 3. Response surfaces for (a) CO_2 and (b) water leakage to the surface as a function of well permeability, CO_2 saturation in the reservoir, and depth of the reservoir at two different injection pressures as a fraction of lithostatic pressure (Π).

water flow with greater flow rates occurring in deeper reservoirs for the same Π, because lithostatic pressure increases at a faster rate than hydrostatic. (For the same *absolute* pressure of water, flow rate decreases as wellbore depth increases because the gradient is less steep and hydrostatic pressure is greater.) Unlike water flow rate, the impact of depth on CO_2 flow rate is relatively small and the relationship between CO_2 flow rate and depth can be either proportional or inversely proportional depending on the other factors. This is because of the complex interactions between CO_2 density and viscosity, and the effect of the volume of gas-phase CO_2 in the wellbore (Section 4.1). For water, the relationship is more straightforward because there is no phase change or buoyancy. Additional discussion of the CO_2 response surfaces is provided in Section 4.2.

3.2. Leakage with an overlying aquifer

Response surfaces for CO_2 and water leakage for Case 2 (with a 500 m thick aquifer at the top of the wellbore) are shown in Fig. 4. In these simulations, leaking fluid was allowed to escape either to an overlying aquifer or to the atmosphere.

A comparison of Figs. 3 and 4 shows the effect of the overlying aquifer. Flow rates are generally higher, both for CO_2 (average of 47% higher) and water leakage (average of 24% higher). The effect of depth and permeability are stronger where the aquifer is present. To illustrate the causes of differences in simulations with and without an overlying aquifer, Fig. 5 shows physical properties of CO_2, including phase changes, for a single realization. Parameters for this case include a wellbore of $k = 8.4 \times 10^{-12}$ m^2 (8.4 darcy) that penetrates a storage reservoir at a $D = 1368$ m below ground surface. In this case, the wellbore effective permeability is greater than the overlying aquifer permeability, which is set to 1×10^{-12} m^2 (1 D) for all simulations. Pressure of CO_2 at the leak point is $\Pi = 0.53$ of lithostatic overburden, which corresponds to an absolute pressure $P = 14.9$ MPa.

Pressure, CO_2 density, and CO_2 viscosity are shown for both the aquifer case (Case 2) and direct atmospheric leakage case (Case 1). The presence of the overlying aquifer increases flow rates from the reservoir: for the same total overall depth, there is a steeper pressure gradient below the aquifer (Fig. 5a) because pressures equilibrate laterally at the base of the aquifer to the fixed hydrostatic far-field boundary. Lower pressures at deeper depths in the wellbore in Case 2 also cause phase change to occur at a deeper depth compared to Case 1, creating a longer column of gaseous CO_2 in the wellbore and thus a stronger excess overpressure for the same pressure of injection (Section 4.1). These effects both contribute to higher flow rates for the case with an overlying aquifer compared to the case without. CO_2 and water leakage for the same realization are shown in Fig. 6; CO_2 leakage rates increased by 48% with the aquifer in this simulation.

Where the wellbore intersects the base of the aquifer, CO_2 in wellbore nodes may flow into the aquifer (as a result of an initial lateral pressure gradient between the wellbore and aquifer) and up the wellbore (as a result of a vertical pressure gradient and buoyancy). At any given location in the wellbore along the aquifer, the difference in pressure gradients in the horizontal and vertical directions, the permeability difference between wellbore and aquifer, and the buoyancy of CO_2 at the aquifer depth all determine the fraction of CO_2 flow that enters the aquifer or continues up the wellbore.

3.3. Response surface fit and validation

Table 2 shows the relative importance of the input parameters for the four MARS response surfaces produced for leakage (CO_2

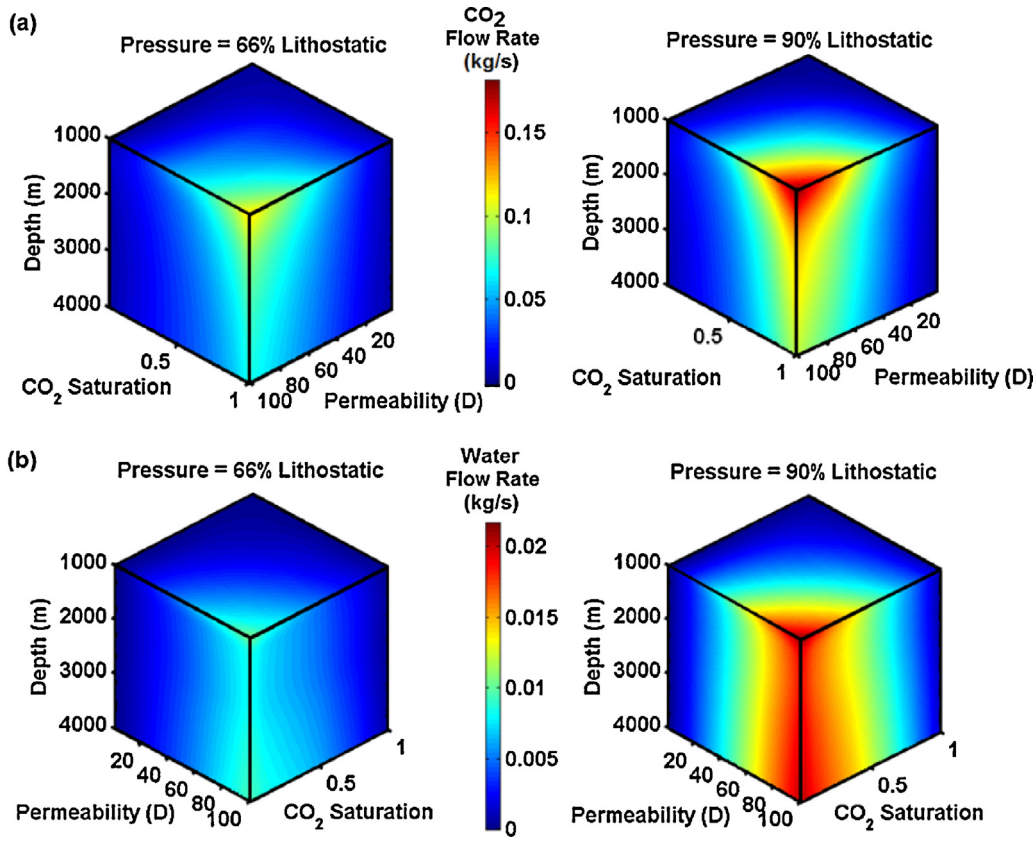

Fig. 4. Response surfaces for (a) CO_2 and (b) water leakage from the reservoir with an overlying aquifer as a function of well permeability, CO_2 saturation in the reservoir, and depth of the reservoir at two different injection pressures (Π).

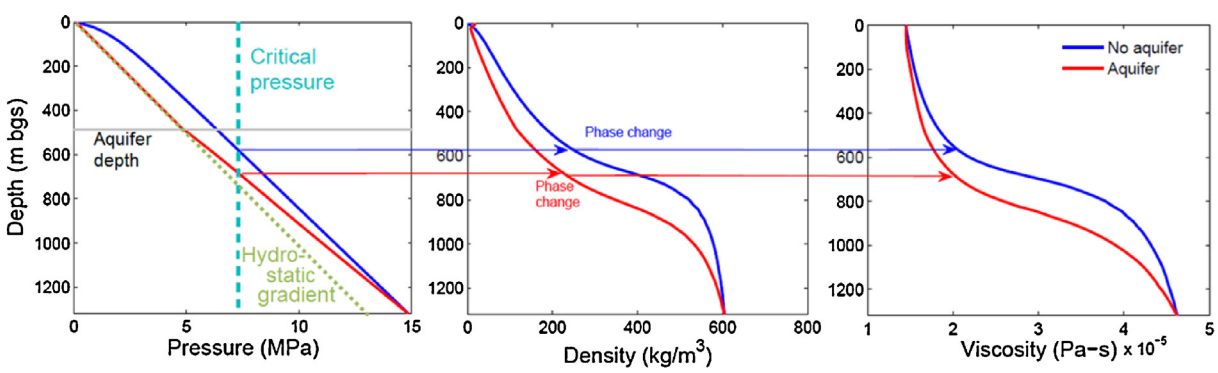

Fig. 5. Physical properties of CO_2 during steady-state leakage in a wellbore with (red) and without (blue) a 500-m thick overlying aquifer as a function of depth below ground surface (bg): (a) pressure, (b) density of CO_2, and (c) viscosity of CO_2.(For interpretation of the references to color in this figure legend, the reader is referred to the web version of this article.)

leakage with no aquifer, CO_2 leakage with a shallow aquifer, water leakage with no aquifer, and water leakage where a shallow aquifer is present). The wellbore permeability k was the most important parameter for all cases. The second most important was C for the CO_2 leakage response surfaces, and Π for the brine leakage models. Depth was ranked fourth for all models. Residual water saturation S_{wr} generally had a minor or negligible effect on the response surface.

The relative importance (in parentheses) is computed by performing cross-validation with each variable individually removed

Table 2
For the four response surfaces, the ranking of importance of each variable to the MARS response surface.

Rank	CO_2 leakage, no aquifer	CO_2 leakage, with aquifer	Brine leakage, no aquifer	Brine leakage, with aquifer
1	k (100.0)	k (100.0)	k (100.0)	k (100.0)
2	C (64.1)	C (65.8)	Π (54.0)	Π (51.4)
3	Π (23.4)	Π (26.9)	C (42.4)	C (47.2)
4	D (5.8)	D (20.3)	D (24.1)	D (6.3)
5	S_{wr} (0.6)	S_{wr} (0.0)	S_{wr} (0.7)	S_{wr} (0.0)

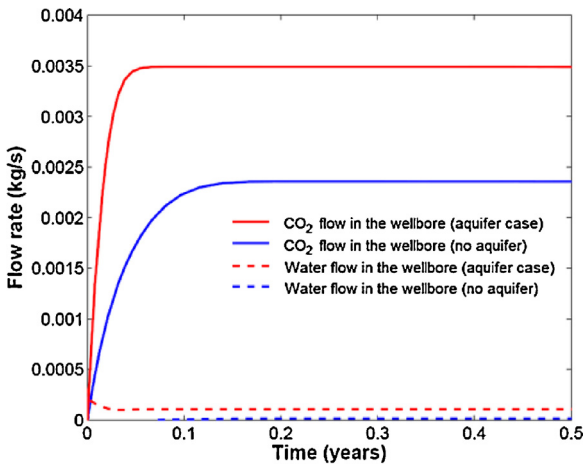

Fig. 6. Flow rates of CO_2 and water up the wellbore in the case with (red) and without (blue) a 500 m overlying aquifer. In the overlying aquifer case, the total flow up the wellbore before the base of the aquifer is shown.(For interpretation of the references to color in this figure legend, the reader is referred to the web version of this article.)

from the computation. The PSUADE software includes several utilities for analyzing the "goodness" of a response surface. The L1-norm or interpolation error is the difference between the interpolated response surface prediction and the output results used to train the response surface. Histograms of the interpolation error, normalized by the data value (flow rate in kg/s), are shown in Fig. 7 for the CO_2 response surfaces (with and without an aquifer) and the water response surfaces. Although there are a very few large outliers on the scaled interpolation error, it can be verified that these correspond to very low flow rates. For example, for Fig. 7a (CO_2 flow rate, no aquifer), all points with relative error greater than 10 (an order of magnitude) correspond to flow rates less than 1.5×10^{-5} kg/s. Interpolation errors for only the points with flow rates greater than 1×10^{-4} kg/s are also shown in Fig. 7 (insets), and they are all less than an order of magnitude.

Table 3
Summary of unscaled errors for the response surfaces.

	Avg. L1-norm (kg/s)	RMS error (kg/s)	Avg. error (kg/s)
CO_2 leakage, no aquifer	1.03E – 04	2.13E – 04	−9.10E – 12
CO_2 leakage, with aquifer	3.26E – 04	4.99E – 04	−6.22E – 10
Water leakage, no aquifer	2.35E – 05	5.37E – 05	5.38E – 11
Water leakage, with aquifer	3.04E – 05	4.32E – 05	−2.54E – 10

Table 3 provides a summary of the unscaled L1-norm, root-mean-square deviation (RMS), and average error of the response surface. Average error is close to zero. The unscaled L1-norm and RMS errors are close to 1×10^{-4} kg/s.

We have also compared the response surface results to full FEHM simulations with data points that were *not* used to generate the surface. A set of 300 randomly generated verification runs were simulated in FEHM. The response surface was then used to predict CO_2 and water leakage for each of those cases based on the parameters depth, permeability, CO_2 saturation, and pressure. Comparisons between CO_2 leakage predicted by the response surface and full FEHM simulations are presented in Fig. 8 for the cases with and without an overlying aquifer. Water leakage is shown in Fig. 9. R^2 values are very good for the match between the response surface ROM and the full FEHM simulations (>0.9964).

The response surface performs worse at low flow rates because competing factors (buoyancy, density and viscosity change, and weight of the column above) become more impactful, causing some of the worst nonlinearities. A second-generation wellbore leakage ROM is in development to handle this region. However, leak rates below 10^{-4} kg/s translate to 3.2 t/yr, which have insignificant impact on storage performance of a sequestration reservoir. For

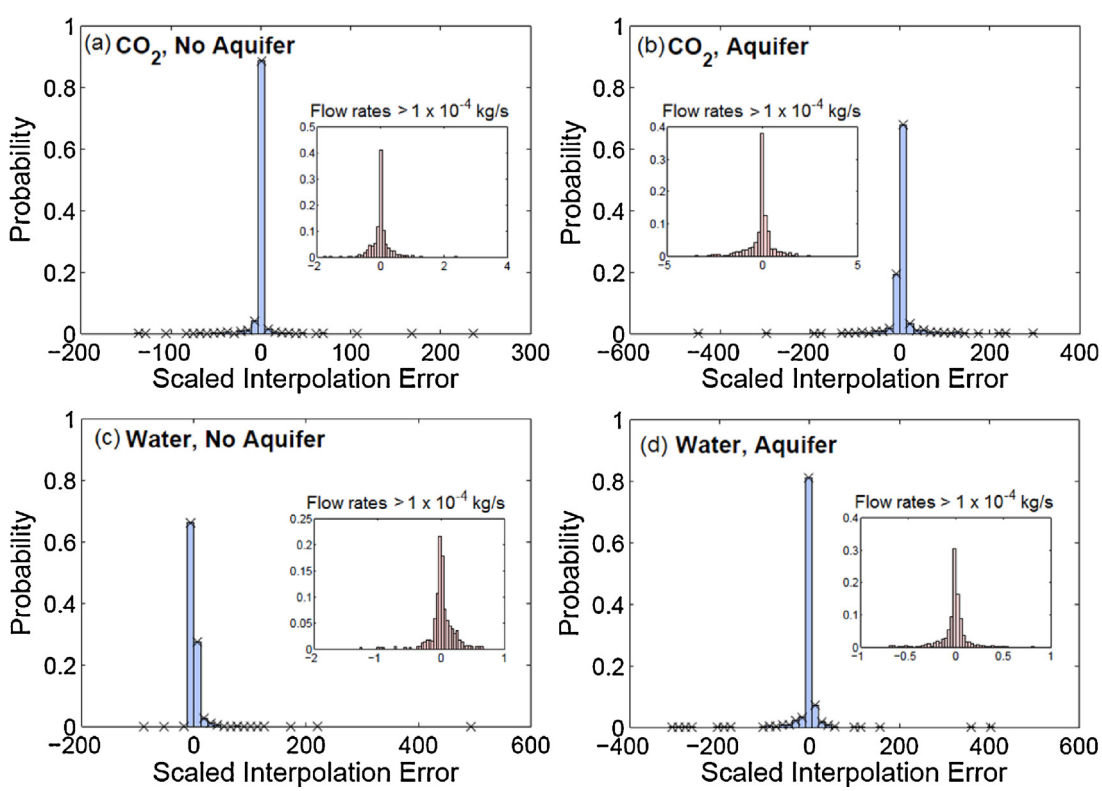

Fig. 7. Relative (scaled) interpolation errors (L1-norm) for the response surfaces for (a) CO_2 with no aquifer; (b) CO_2 with a shallow aquifer; (c) water with no aquifer; and (d) water with an aquifer. Inset histograms show the same error for all points with flow rates greater than 1×10^{-4} kg/s.

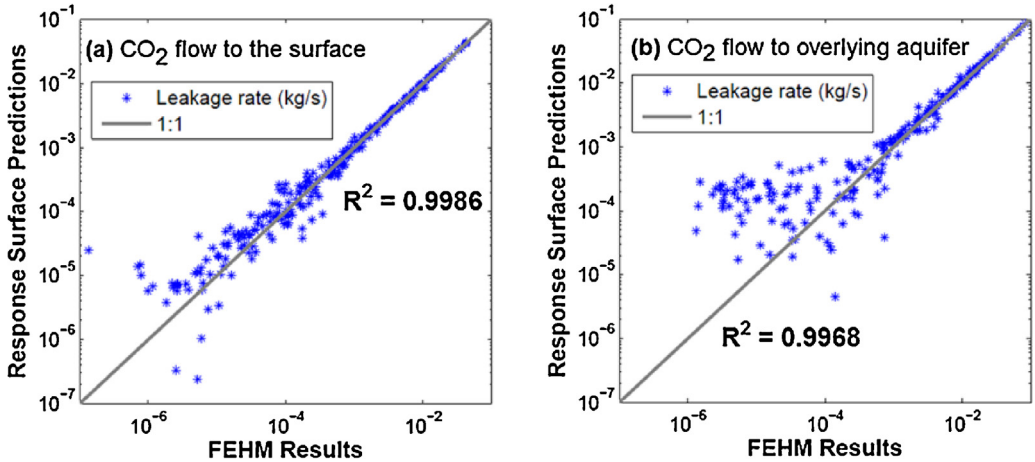

Fig. 8. Performance of the response surface for predicting CO_2 leakage as compared to full FEHM simulations for (a) the case with leakage to the surface and (b) leakage to a 500 m overlying aquifer.

example, injection at 1 MT/year and leakage at 10^{-4} kg/s would mean losses of 0.00032% per year, which falls well below 0.1% per year (UNFCCC, 2006). We use a conservative approach in CO_2-PENS and set leak rates predicted below 10^{-4} kg/s to 10^{-4} kg/s. The impact of CO_2 leakage on groundwater resources using the response surfaces developed here is explored in Dai et al. (2014) and Carroll et al. (2014).

4. Discussion

The approach taken here differs from other methods for estimating wellbore leakage because the of the use of a multiphase flow and transport simulator that takes into account the complex processes, including phase change of CO_2, to develop ROMs for large-scale probabilistic risk analysis applications, as compared to analytical or semi-analytical models for leakage that have typically been used for this in the past (Celia and Nordbotten, 2011; Nordbotten et al., 2004, 2005). Thus, the response surface reflects complex nonlinear flow effects and the phase change from dense (liquid or supercritical) to gaseous CO_2 in the upper portions of the wellbore. Our method does not have the simplifications found in many prior techniques used to estimate leakage analytically (e.g., single-phase flow, constant density and viscosity of CO_2) (Viswanathan et al., 2008), yet it can provide leakage estimates for thousands of realizations in a performance assessment model in a fraction of the time that it would take to run the same number of multiphase reservoir simulations.

4.1. Effect of increased overpressure on flow rate at shallow depths

When considering the effect of CO_2 pressure on leakage rate and applying Darcy's Law, it is tempting to assume that an increased absolute pressure of injection, P, will result in an increased flow rate. However, in certain regimes, this is not the case. For example, in Fig. 10 simulations are shown with fixed parameters except for Π (which varies uniformly from 0.485–0.90, with 0.485 corresponding to hydrostatic pressure for the given conditions), with the reservoir located at three depths (1000, 1500, and 3000 m below ground surface). The steady state CO_2 leakage rate is shown in the figure. For the shallowest simulations, an increase in pressure initially causes a decrease in CO_2 leakage rates (note that, for a given depth, an increase in Π is an increase in absolute pressure). After a turning point, increased pressure leads to increased leakage rate, as expected. Fig. 7b shows the same curves as a function of excess pore pressure (*EPP*), another standard metric used to describe

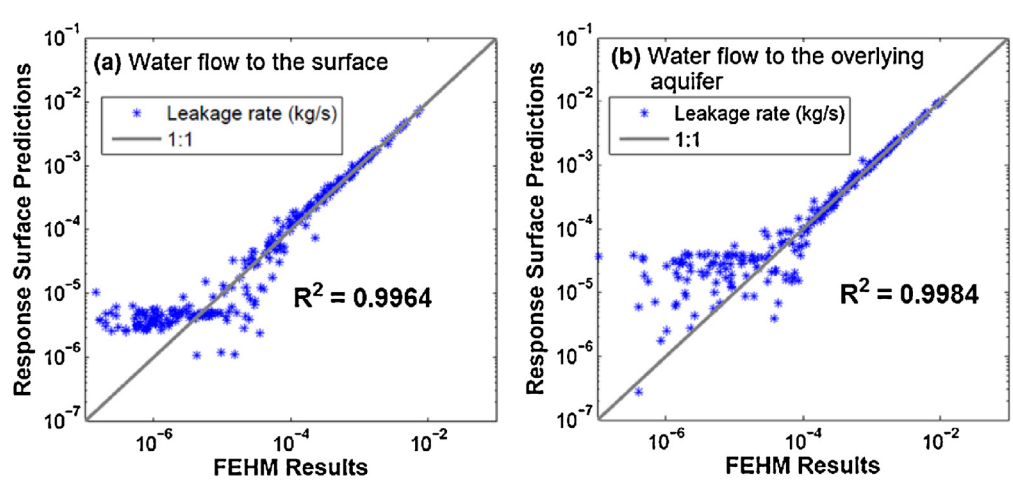

Fig. 9. Performance of the response surface for predicting water leakage as compared to full FEHM simulations for (a) the case with leakage to the surface and (b) leakage to a 500 m overlying aquifer.

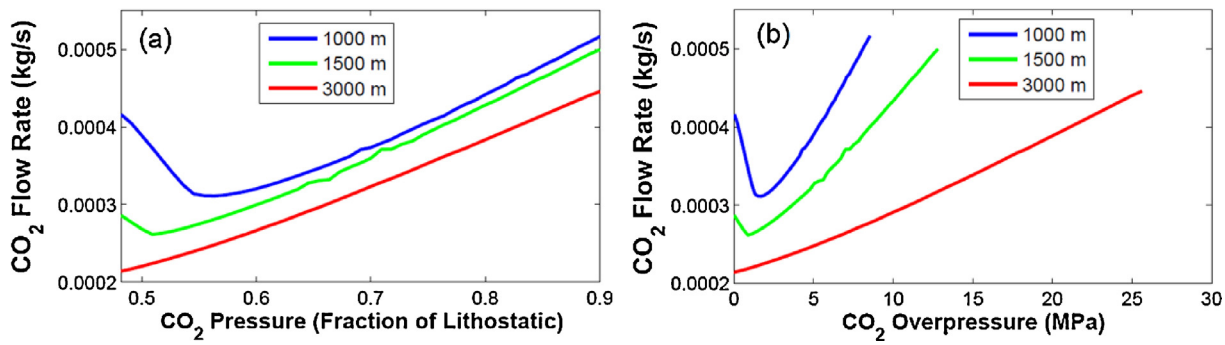

Fig. 10. Flow rate of CO_2 up a leaking wellbore for simulations with varying injection pressure, with pressure represented as (a) fraction of lithostatic overburden pressure at each particular depth (Π) and (b) *EPP*, the overpressure of CO_2 compared to reservoir pressure (hydrostatic).

overpressures of CO_2 injection. *EPP* is pressure relative to initial hydrostatic pressure in the wellbore, $EPP = P_{\text{pore}} - P_{\text{hydrostatic}}$ (e.g., Stauffer and Bekins, 2001).

The cause of the turning point is the effect of the actual weight of the CO_2 gas/liquid column above the wellbore/reservoir intersection when determining excess pressure. For a vertical cylindrical wellbore composed of a porous medium of homogeneous properties stretching from the reservoir to the surface, the mass flow rate Q_m for CO_2 and water based on the multiphase form of Darcy's Law is related to the area of the leakage pathway, the actual excess pore pressure gradient in the wellbore, the density and viscosity of CO_2 and brine, the effective permeability of the wellbore (ignoring internal heterogeneity of the wellbore), the relative permeabilities of the fluids, and the saturation of CO_2 and water. The actual excess pressure of interest is not the pressure of the CO_2 (P), or *EPP* as shown in Fig. 10b, but pressure due to the weight of the multiphase CO_2 column. After CO_2 leakage has been occurring for some time, the wellbore column contains a mixture of CO_2 (in various phases) and the nonwetting phase, water. In our model containing a column of discrete cells of height Δz_i, we define the excess pore pressure relative to hydro/CO_2-static pressure (EPP^*) as:

$$EPP* = P - g\sum_{i=1}^{N}\left(\rho_{g,i}S_{g,i} + \rho_{l,i}S_{l,i}\right)\ \Delta z_i, \tag{4}$$

where $\rho_{x,i}$ is the density of phase x (g—gaseous CO_2; l—liquid or supercritical CO_2) and $S_{x,i}$ is the fractional saturation of phase x in wellbore cell i, g is acceleration due to gravity, and N is the number of nodes in the wellbore.

By Darcy's Law, the mass flow rate of phase x in the simple wellbore depends on the gradient of EPP^*:

$$Q_m = -\rho_x \mathrm{A} \mathrm{R}_x \frac{k}{\mu_x}\left(\nabla EPP*\right), \tag{5}$$

which may be applied over small segments of the wellbore with constant density and viscosity. As before, x represents a fluid phase, either water (w), liquid or supercritical CO_2 (l), or gaseous CO_2 (g). The matrix permeability is k, μ_x is the viscosity of each phase, and R_x is the relative permeability for each phase.

Fig. 11 shows CO_2 flow rate versus *EPP*, EPP^* (Eq. (4)), and $EPP^*\rho_l/\mu_l$ (where ρ_l and μ_l are supercritical CO_2 density and viscosity at the point of CO_2 leakage into the wellbore). Other factors in Eqs. (4) and (5) are not varied between simulations (A, k, Δz). The relative permeability factor, R_x, will differ somewhat based on final saturations of the phases in the wellbore, but it does not make a significant difference. Therefore, the bottom plot (Fig. 8c) contains the factors that are expected to influence flow rate, and the result is an almost linear response of the flow rate to the variable $EPP^*\rho_l/\mu_l$.

Thus, the initially non-intuitive result that increased overpressure leads to a decrease in flow rate (at the same depth) can be seen to have a simple cause. Higher pressure causes the CO_2 phase change to gas to occur at a shallower depth, and less overlying gas causes greater weight of the CO_2 above, leading to reduced flow for greater pressure. The effect is also coupled with the buoyancy drive of a CO_2 parcel in the wellbore, as buoyancy depends on the pressure gradient of the surrounding fluid.

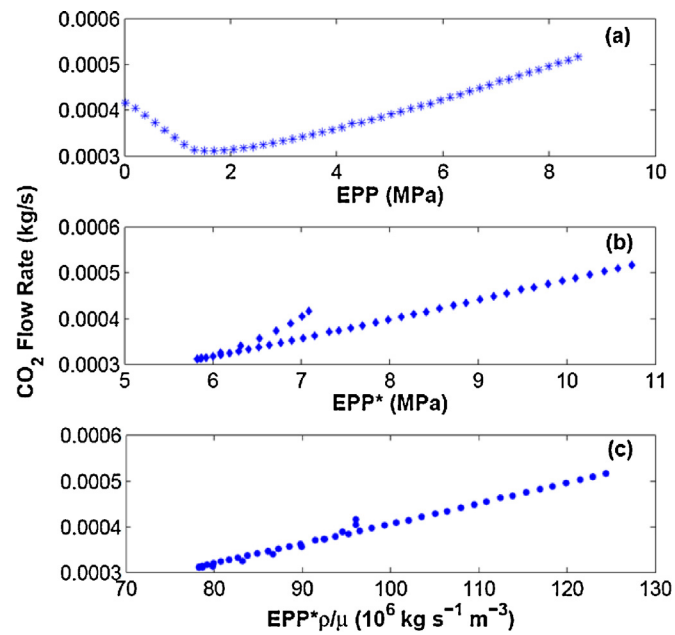

Fig. 11. Leakage rates in the wellbore for simulations with fixed depth (1000 m) and varying Π, from 0.485 (in this case, hydrostatic; $P = 9.8$ MPa, $EPP = 0$) to 0.90 ($P = 18.3$ MPa, $EPP = 8.5$ MPa). (a) CO_2 leakage rate versus *EPP* (excess pore pressure relative to initial hydrostatic pressure). The non-monotonic response is caused by changing volumes of CO_2 phases in the wellbore. (b) Flow rate versus EPP^* (Eq. (4)). (c) Flow rate versus $EPP^*\rho_l/\mu_l$ (Eq. 5).

4.2. Response surface features

The effect discussed in Section 4.1 is just one cause of complexity in the CO_2 leakage ROM. Slices through the 4-D response surfaces for CO_2 (Figs. 12–14) show interesting features in this nonlinear, multiphase system with supercritical, liquid, and gaseous CO_2, and water. Reversals and inflection points in the response surface are what drive the necessity of using the MARS fitting algorithm, as opposed to a multivariate polynomial regression. The cause of reversals and inflection points in the CO_2 response surfaces is the complex interplay between driving forces for leakage (buoyancy, pressure gradient), and fluid properties (density, viscosity, enthalpy) for a particular pressure and temperature regime, phase

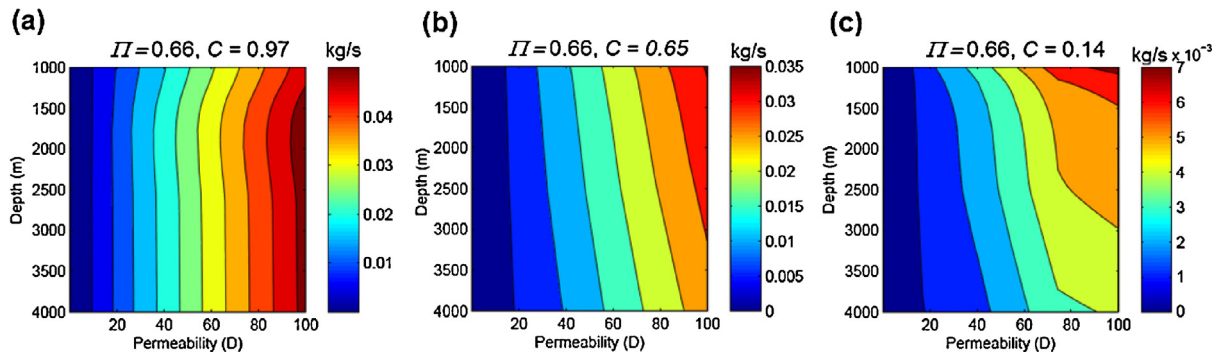

Fig. 12. Slices through the CO_2 leakage response surface, no aquifer, at a fixed $\Pi = 0.66$ at three different saturations of CO_2 (0.97, 0.65, and 0.14).

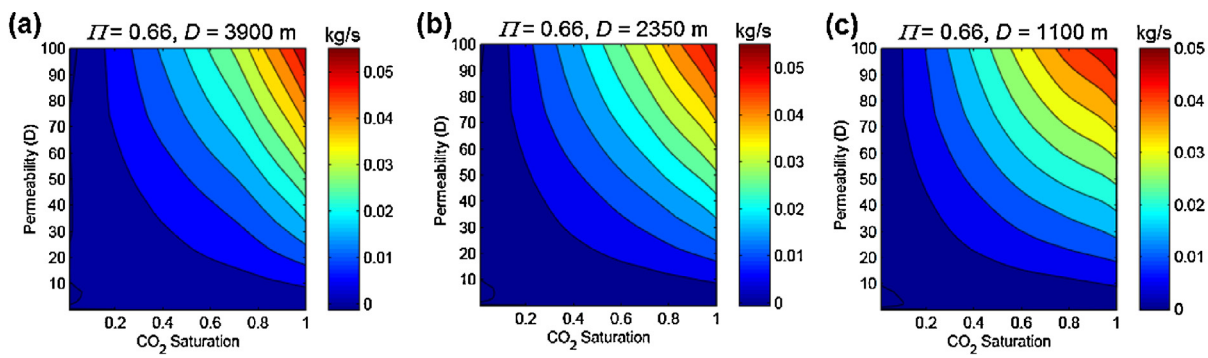

Fig. 13. Slices through the CO_2 leakage response surface, no aquifer, at a fixed $\Pi = 0.66$ at three different depths (3900, 2350, and 1100 m).

mobilities based on saturation (relative permeabilities of CO_2 and water). Below, slices showing interesting features are presented along with discussion of the other input parameters (k, C, and D), in addition to Π which was discussed in Section 4.1.

Fig. 12 shows slices through the CO_2 leakage response surface (no aquifer) at three different permeabilities, for a fixed $\Pi = 0.66$ (that is, regardless of depth, pressure of injection is 66% of lithostatic pressure; actual overpressure can be calculated from Eq. (1)). The effect of permeability is generally straightforward–higher permeabilities lead to higher leakage rates.

In Fig. 13, slices are shown for fixed $\Pi = 0.66$, at three depths, with varying C and k. It is clear that both C and k have a strong and direct impact on flow rate. The different depths have little effect in this case.

At low permeabilities, where flow rates are small, other factors begin to dominate the Darcy flux (Eq. (5)), such as the phase change effect discussed in Section 4.1. For example, Fig. 14 shows a reversal of flow rate with pressure as permeability decreases. There is a critical permeability at which the effect of pressure on flow rate changes direction: at high permeabilities (>1.1 D), increasing pressure generally causes an increase in flow rate, but at low permeabilities, increasing Π causes a decrease in flow rate (note, again, that for a fixed depth, an increase in Π is a direct increase in absolute pressure).

4.3. Case study: Wellbore leakage ROMs in CO_2-PENS

The use of ROMs created from the response surfaces is demonstrated in a GCS probabilistic leakage simulation for a hypothetical CO_2 sequestration operation. The reservoir model is based on the Kimberlina site in central California (Birkholzer et al., 2011b). We assume that there are five legacy wellbores that are cemented and the cement permeabilities are randomly drawn from a user-defined truncated lognormal distribution with a mean of 3×10^{-12} m^2. Wellbores intersected the CO_2 reservoir at depths of ~2500 m bg (below ground surface; depending on location in the reservoir) and

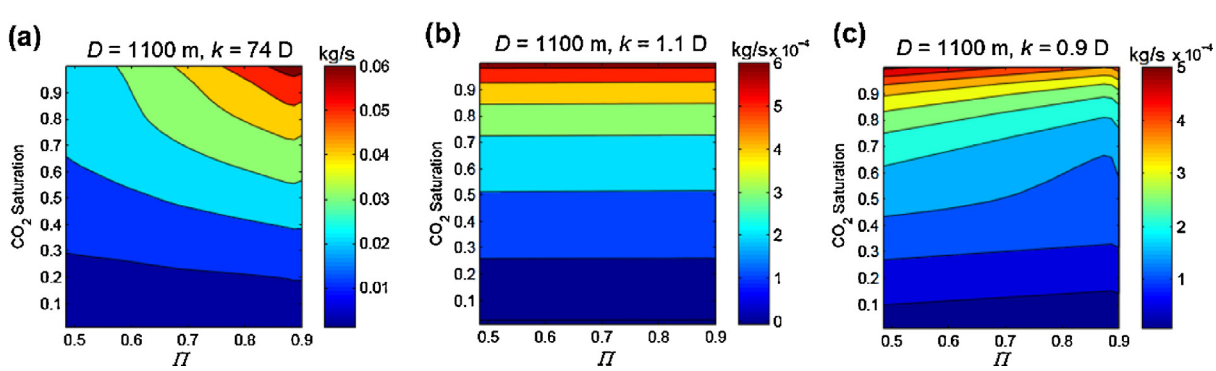

Fig. 14. Slices through the CO_2 leakage response surface, no aquifer, at a fixed depth = 1100 m at three different permeabilities (74, 1.1, and 0.9 D). At high permeabilities (a), flow rate increases with pressure as a fraction of lithostatic (Π) for a fixed depth; at around $k = 1$ D there is a reversal and flow rate decreases with increasing Π at lower permeabilities (c).

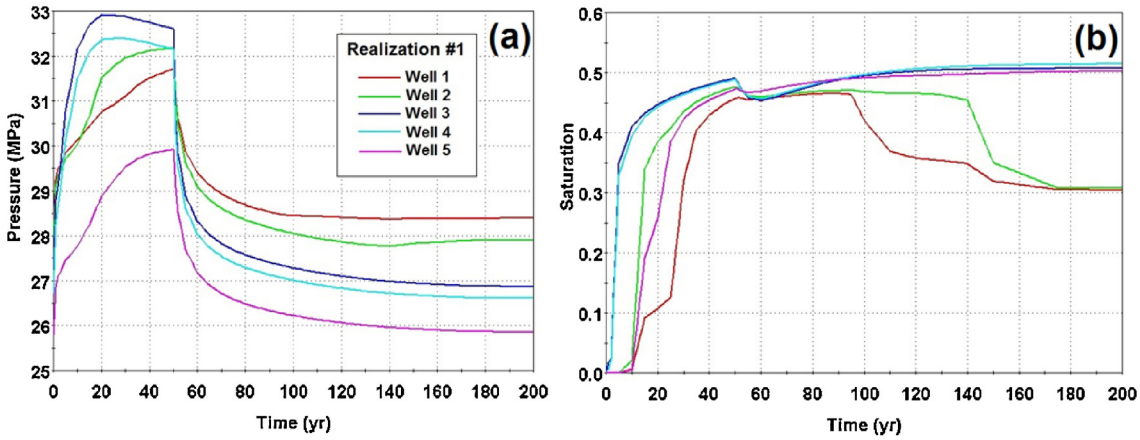

Fig. 15. (a) CO_2 pressure and (b) saturation at five leaky wells for one realization of the CO_2-PENS Kimberlina simulations.

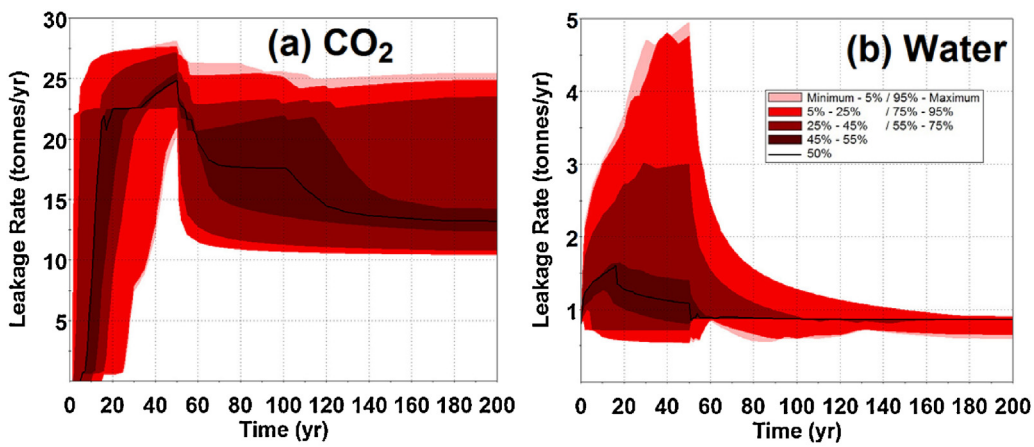

Fig. 16. Ensemble statistics across 50 realizations for (a) CO_2 and (b) water leak rate at well 1 in the CO_2-PENS Kimberlina simulations. Envelopes represent flow rates for various proportions of realizations.

Table 4
Injection and legacy well coordinates for the Kimberlina simulation.

Well	*X*-coordinate (m)	*Y*-coordinate (m)	Distance from injector (m)
Injector	37,000	48,500	–
Well 1	35,500	49,200	1655
Well 2	36,600	49,200	806
Well 3	37,000	49,200	700
Well 4	37,500	49,200	860
Well 5	38,500	49,200	1655

intersected a shallow aquifer (50 m bg to ground surface). The five legacy wells are situated along a line trending east/west, 650 m north of the injector well (Table 4). Note that this configuration is used only for demonstrating applicability of the wellbore leakage ROM in CO_2-PENS, and it does not represent a specific set of wells at the Kimberlina site.

The underlying reservoir model in this CO_2-PENS simulation samples CO_2 pressures and saturations from a set of 54 full reservoir simulations of CO_2 injection into the Kimberlina reservoir. Those 3-D numerical simulations included complex geology and topography (Birkholzer et al., 2011b), although plume evolution can also be modeled analytically within the CO_2-PENS framework instead (CO_2-PENS is modular). CO_2 saturations and pressures at the five legacy wellbores in CO_2-PENS for one realization (out of 50) are shown in Fig. 15.

Ensemble statistics for leakage from one well (legacy Well 1, 1655 m from the injector) for all 50 CO_2-PENS realizations are shown in Fig. 16. What varies between each of the 50 CO_2-PENS realizations is (1) wellbore permeability and (2) CO_2 saturation and pressure at the leak point location over time (drawn from one of the 54 full reservoir simulations). In this region of the response surface, CO_2 leakage rate is more sensitive to CO_2 saturation than the range of overpressure, while water leakage rate is more sensitive to pressure. From the five leaky wellbores in this hypothetical simulation, the mean loss rate of CO_2 of the total 250 MT injection is 0.035%/yr, well below 0.1% per year leakage from GCS sites (UNFCCC, 2006).

Although hypothetical, this result shows the utility of the wellbore leakage ROM in being able to quickly quantify the impact of potential leaking wells in a complex system-level risk analysis. The ROM embedded in CO_2-PENS can run 50 realizations in 10 min on a 2.7 GHz computer, whereas running full-physics multiphase reservoir simulations of this system on the same machine takes significantly longer.

5. Conclusions

The response surface approach to estimating wellbore leakage is a straightforward, direct technique that is constructed from multiphase porous flow and transport numerical simulations and is used for quick turn-around-time analyses of multiple wellbores across many realizations in a system-level model. Simplifying assumptions required in analytical solutions are not required here, while the computational effort of estimating leakage in regional-scale numerical simulations is eliminated from the run-time of the

uncertainty analysis. The nonlinear, coupled responses to varying input parameters that make CO_2 and brine leakage estimation difficult to solve analytically are accounted for by the multiphase flow and transport simulator FEHM. We model the wellbore as a porous medium in which the nature of the leakage pathway is not known, but an effective permeability is assigned to the wellbore as an equivalent Darcy medium. The response surface also handles varying reservoir depth, and the pressure and saturation of CO_2 at the leak point are the other input parameters for determining leakage rate from the storage reservoir.

A spline-fitting algorithm (MARS) was used to build a ROM of the response surface using an LHS sampling scheme in FEHM simulations. The fitting of the response surface to a discrete suite of Monte Carlo simulations with highly sensitive outputs due to nonlinearities in the flow problem introduces errors in the estimates, so the response surface performance was tested against the full-complexity FEHM simulations to ensure its reliability within the relevant parameter ranges.

In one set of sensitivity tests, the pressure at the leak point was varied from 48.5% lithostatic to 90% lithostatic pressure for depths of 1000, 1500, and 3000 m. The resulting leakage rates suggest a counter-intuitive decrease in flow for an increase in pressure at the shallower depths. The effect is a result of gas formation in the top of the wellbore, where higher pressures *shorten* the length of gas column in the wellbore, resulting in a heavier column above and thus a lower actual excess pore pressure (*EPP**). The implication for shallow reservoirs is that an increase in reservoir pressure may cause a decrease in wellbore leakage for wellbores that do not release CO_2 to aquifers. For deep wellbores, the fraction of the wellbore that is composed of CO_2 gas is small compared to the fraction that is in a denser phase, and increases in pressure lead to the expected increases in flow rate.

The results of this study contribute towards the effort to predict wellbore leakage before GCS is tested on a sufficiently large scale to generate real field data on leakage. However, this method provides a defensible estimate of leakage when implemented in a probabilistic framework that samples across a wide range of the most relevant uncertain parameter, the effective wellbore permeability. The method may be easily adapted to generate response surfaces for wellbore leakage within alternate conceptual scenarios (e.g., thief zones) if some site-specific geologic information is known. The method may also be used with simulators that include additional physical processes in the CO_2/brine leakage system (e.g., geochemical reactions).

Acknowledgements

This work was funded by the U.S. Department of Energy under the Advanced Carbon Capture and Storage Simulation Initiative through the National Risk Assessment Partnership (NRAP), under grant DE-AC52-06NA25396. The authors would like to thank two anonymous reviewers, whose comments greatly improved this paper.

References

Bachu, S., 2000. Sequestration of CO_2 in geological media: criteria and approach for site selection in response to climate change. Energy Convers. Manage. 41 (9), 953–970.

Bachu, S., Bennion, B., 2008. Effects of in-situ conditions on relative permeability characteristics of CO_2-brine systems. Environ. Geol. 54 (8), 1707–1722.

Bachu, S., Bennion, B., 2009. Interfacial tension between CO_2, freshwater, and brine in the range of pressure from (2 to 27) MPa, temperature from (20 to 125) °C, and water salinity from (0 to 334,000) mg L^{-1}. J. Chem. Eng. Data 54 (3), 765–775.

Balashov, V.N., Guthrie, G.D., Hakala, J.A., Lopano, C.L., Rimstidt, J.D., Brantley, S.L., 2013. Predictive modeling of CO_2 sequestration in deep saline sandstone reservoirs: impacts of geochemical kinetics. Appl. Geochem. 30, 41–56.

Birkholzer, J.T., Nicot, J.P., Oldenburg, C.M., Zhou, Q., Kraemer, S., Bandilla, K., 2011a. Brine flow up a well caused by pressure perturbation from geologic carbon sequestration: Static and dynamic evaluations. Int. J. Greenhouse Gas Control 5 (4), 850–861.

Birkholzer, J.T., Zhou, Q., Cortis, A., Finsterle, S., 2011b. A sensitivity study on regional pressure buildup from large-scale CO_2 storage projects. Energy Procedia 4, 4371–4378.

Brunet, J.-P.L., Li, L., Karpyn, Z.T., Kutchko, B.G., Strazisar, B., Bromhal, G., 2013. Dynamic evolution of cement composition and transport properties under conditions relevant to geological carbon sequestration. Energy Fuels 27 (8), 4208–4220.

Carey, J.W., 2013. Geochemistry of wellbore integrity in CO_2 sequestration: portland cement-steel-brine-CO_2 interactions. Rev. Mineral. Geochem. 77 (1), 505–539.

Carey, J.W., Wigand, M., Chipera, S.J., WoldeGabriel, G., Pawar, R.J., Lichtner, P.C., Wehner, S.C., Raines, M.A., Guthrie Jr., G.D., 2007. Analysis and performance of oil well cement with 30 years of CO_2 exposure from the SACROC Unit, West Texas, USA. Int. J. Greenhouse Gas Control 1 (1), 75–85.

Carroll, S.A., Keating, E., Mansoor, K., Dai, Z., Sun, Y., Trainor-Guitton, W., Brown, C., Bacon, D., 2014. Key factors for determining groundwater impacts due to leakage from geologic carbon sequestration reservoirs. Int. J. Greenhouse Gas Control 29, 153–168.

Celia, M.A., Nordbotten, J.M., 2011. How simple can we make models for CO_2 injection, migration, and leakage? Energy Procedia 4, 3857–3864.

Crow, W.J., Carey, J.W., Gasda, S.E., Williams, D.B., Celia, M., 2010. Wellbore integrity analysis of a natural CO_2 producer. Int. J. Greenhouse Gas Control 4 (2), 186–197.

Dai, Z., Keating, E., Bacon, D., Viswanathan, H., Stauffer, P., Jordan, A., Pawar, R., 2014. Probabilistic evaluation of shallow groundwater resources at a hypothetical carbon sequestration site. Sci. Rep. 4, 1–7.

Dash, Z.V., 2003. Validation Test Plan for the FEHM Application. Los Alamos National Lab, ⟨https://fehm.lanl.gov/pdfs/fehm_vvp.pdf⟩ (accessed 26 August 2014) Version 2.21. Rep. 10086-VTP-2.20-00.

Dempsey, D., Kelkar, S., Pawar, R., Keating, E., Coblentz, D., 2014. Modeling caprock bending stresses and their potential for induced seismicity during CO_2 injection. Int. J. Greenhouse Gas Control 22, 223–236.

Deng, H., Stauffer, P.H., Dai, Z., Jiao, Z., Surdam, R.C., 2012. Simulation of industrial-scale CO_2 storage: multi-scale heterogeneity and its impacts on storage capacity, injectivity and leakage. Int. J. Greenhouse Gas Control 10, 397–418.

Friedman, J.H., 1991. Multivariate adaptive regression splines. Ann. Stat. 19 (1), 1–141.

Gasda, S.E., Nordbotten, J.M., Celia, M.A., 2008. Determining effective wellbore permeability from a field pressure test: a numerical analysis of detection limits. Environ. Geol. 54, 1207–1215.

Gasda, S.E., Bachu, S., Celia, M., 2004. Spatial characterization of the location of potentially leaky wells penetrating a deep saline aquifer in a mature sedimentary basin. Environ. Geol. 46, 707–720.

Hu, L., Pan, L., Zhang, K., 2012. Modeling brine leakage to shallow aquifer through an open wellbore using T2WELL/ECO2N. Int. J. Greenhouse Gas Control 9, 393–401.

Metz, B., Davidson, O., de Coninck, H., Loos, M., Meyer, L., 2005. PCC special report on carbon dioxide capture and storage. In: Intergovernmental Panel on Climate Change, ⟨http://www.ipcc.ch/activity/srccs/index.htm⟩.

Linstrom, P.J., Mallard, W.G. (Eds.), 2014. NIST Chemistry WebBook. NIST Standard Reference Database Number 69. National Institute of Standards and Technology, Gaithersburg, MD, ⟨http://webbook.nist.gov⟩ (accessed 2 September 2014).

Middleton, R.S., Keating, G.N., Stauffer, P.H., Jordan, A.B., Viswanathan, H.S., Kang, Q.J., Carey, J.W., Mulkey, M.L., Sullivan, E.J., Chu, S.P., Esposito, R., Meckel, T.A., 2012. The cross-scale science of CO_2 capture and storage: from pore scale to regional scale. Energy Environ. Sci. 5 (6), 7328–7345.

Nordbotten, J.M., Celia, M.A., Bachu, S., 2004. Analytical solutions for leakage rates through abandoned wells. Water Resour. Res. 40 (4).

Nordbotten, J.M., Kavetski, D., Celia, M.A., Bachu, S., 2009. Model for CO_2 leakage including multiple geological layers and multiple leaky wells. Environ. Sci. Technol. 43 (3), 743–749.

Nordbotten, J.M., Celia, M.A., Bachu, S., Dahle, H.K., 2005. Semianalytical solution for CO_2 leakage through an abandoned well. Environ. Sci. Technol. 39 (2), 602–611.

Pan, L., Oldenburg, C.M., Wu, Y.K., 2009. Wellbore flow model for carbon dioxide and brine. Energy Procedia 1 (1), 71–78.

Pan, L., Oldenburg, C.M., Pruess, K., Wu, Y., 2011. Transient CO_2 leakage and injection in wellbore-reservoir systems for geologic carbon sequestration. Greenhouse Gases: Sci. Technol. 1 (4), 335–350.

Pawar, R., Bromhal, G., Dilmore, R., Foxall, B., Jones, E., Oldenburg, C., Stauffer, P., Unwin, S., Guthrie, G., 2013. Quantification of risk profiles and impacts of uncertainties as part of US DOE's National Risk Assessment Partnership (NRAP). Energy Procedia 37, 4765–4773.

Stauffer, P.H., Bekins, B.A., 2001. Modeling consolidation and dewatering near the toe of the northern Barbados accretionary complex. J. Geophys. Res. 106, 6369–6383 (B4).

Stauffer, P.H., Viswanathan, H.S., Pawar, R.J., Guthrie, G.D., 2009. A system model for geologic sequestration of carbon dioxide. Environ. Sci. Technol. 43 (3), 565–570.

Tong, C., 2010. PSUADE Reference Manual (Version 1.3.0). Lawrence Livermore National Laboratory, Livermore, CA, May.

United Nations Framework Convention on Climate Change (UNFCCC), 2006. Annex to the Report of the 26th Meeting of the Executive Board—Recommendation on CO_2 capture and storage as CDM project activities based on the review of cases NM0167. United Nations Framework Convention on Climate

Change (UNFCCC), ⟨https://cdm.unfccc.int/EB/026/eb26_repan13.pdf⟩ (accessed 2 September 2014) NM0168 and SSC_038.

Viswanathan, H.S., Pawar, R.J., Stauffer, P.H., Kaszuba, J.P., Carey, J.W., Olsen, S.C., Keating, G.N., Kavetski, D., Guthrie, G.D., 2008. Development of a hybrid process and system model for the assessment of wellbore leakage at a geologic CO_2 sequestration site. Environ. Sci. Technol. 42 (19), 7280–7286.

Viswanathan, H., Dai, Z., Lopano, C., Keating, E., Hakala, J.A., Scheckel, K.G., Zheng, L., Guthrie, G.D., Pawar, R., 2012. Developing a robust geochemical and reactive transport model to evaluate possible sources of arsenic at the CO_2 sequestration natural analog site in Chimayo, New Mexico. Int. J. Greenhouse Gas Control 10, 199–214.

Yang, C., Prasher, S.O., Lacroix, R., Kim, S.H., 2003. A multivariate adaptive regression splines model for simulation of pesticide transport in soils. Biosyst. Eng. 86 (1), 9–15.

Zyvoloski, G.A., 2007. FEHM: a control volume finite element code for simulating subsurface multi-phase multi-fluid heat and mass transfer. In: Rep. LAUR-07-3359. Los Alamos Natl. Lab., Los Alamos, NM.